Indonesian Journal of Electrical Engineering and Computer Science
Vol. 29, No. 1, January 2023, pp. 295~303
ISSN: 2502-4752, DOI: 10.11591/ijeecs.v29.i1.pp295-303

Hyperspectral image classification using Hyb-3D convolution neural network spectral partitioning

Easala Ravi Kondal, Soubhagya Sankar Barpanda
School of Computer Science and Engineering, VIT-AP University, Amaravati, India

Article Info

Article history:

Received Apr 26, 2022
Revised Sep 15, 2022
Accepted Sep 29, 2022

Keywords:

Convolution neural networks
Deep learning
Hybrid 3D-CNN
Hyperspectral image
Spectral-spatial signature

ABSTRACT

Hyperspectral image classification (HSIC) on remote sensing imaging has brought immersive achievement using artificial intelligence technology. In deep learning convolution neural networks (CNN), 2D-CNN, and 3D-CNN methods are widely used to classify the spectral-spatial bands of hyperspectral images (HSI). The proposed Hybrid 3D-CNN (H3D-CNN) model framework for deeper features extraction predicts classification accuracy in supervised learning. The model reduces the narrow gap between supervised and unsupervised learning and the complexity and cost of the previous models. The HSI classification analysis is carried out on real-world data sets of Indian pines Salinas datasets captured by Airborne visible, infrared imaging spectrometer (AVIRIS) sensors that performed superior classification accuracy results.

Corresponding Author:

Easala Ravi Kondal
School of Computer Science and Engineering, VIT-AP University
Amaravati, Andhra Pradesh, India
Email: easala.ravi@vitap.ac.in

1. INTRODUCTION

Hyperspectral imaging (HSI) research has exploded in recent years due to its wide range of applications. Remote sensing takes digital images with hundreds and thousands of tiny spectral bands with spectral fingerprints ranging from visible to near-visible wavelengths [1]. Remote sensors produce spectrometers images that are rich in spectral and spatial information, and also images are in the form of data cubes with multi-resolution spectral-spatial information of hyperspectral cubes Figure 1 [2], the HSI has been widely applied in agriculture, environmental studies, biological, fraud detection, astronomy, and mineral exploration [3] over the recent decades. Instead of characteristics directly connected to the pixels, each pixel in HSI relies on features from a tiny area surrounding the pixels. In the context of supervised training and classification [4], a variety of methods have been used for HSI data classification multinomial logistic regression [5], support vector machine (SVM), distance measures, K-nearest neighbor, and maximum likelihood [6].

Methods of spectral-spatial categorization can be into two categories spectral and spatial contextual information. Advanced spatial extraction is achieved using morphological profiles [7], entropy [8], attribute profiles [9], and low-rank representation [10]. Then, using dimensionality reduction (DR), these altered spatial data are coupled with spectral features to conduct pixes-wise classification. Furthermore, the Hopfield neural network in [11] has collected hyperspectral data in remote sensing images. The presentation of HSI data in 3D cubes leads to many feature cubes carrying crucial information on signal space [12], spectrum, and combined spatial/spectrum correlation, all of which are necessary for improved perforation.

According to the existing literature, the convolution neural network has gained popularity due to 2D-CNN and 3D-CNN in HSI [13]. Previous models are used for spectral learning, while subsequent models learn local spatial features at each strip [14]. These models exhibit a weakness in feature extraction when applied to multi-dimensional data cubes. The 3D-CNN approach was overly complex due to the calculation and classification accuracy. Non-linear problems can use kernel-based methods as well. By mapping the original data onto a higher-dimensional Hilbert space, kernel techniques convert non-linear problems to linear problems.

In this work, I propose a novel deep learning method for providing a relatively general and comprehensive overview of the existing methods. The motivation of our work is the classification of a hyperspectral image called a hybrid 3D-CNN with enhanced features, which considers both spectral and spatial information. The silent feature of the proposed H3D-CNN model is efficient in hyperspectral image computing and accurate in classification.2D-CNN and 3D-CNN alone are not able to extract accuracy features from the HSI [15], volumetric data with multi-dimensional features [16], [17]. So, this motivates me to propose the Hybrid 3D-CNN. The resulting deep classifier model is trained in an end-to-end. At the same time, the Hybrid 3D-CNN parameters are supervised learning based with a limited number of training samples to increase the accuracy with large testing samples. We compared our model with different real-world HSI datasets.

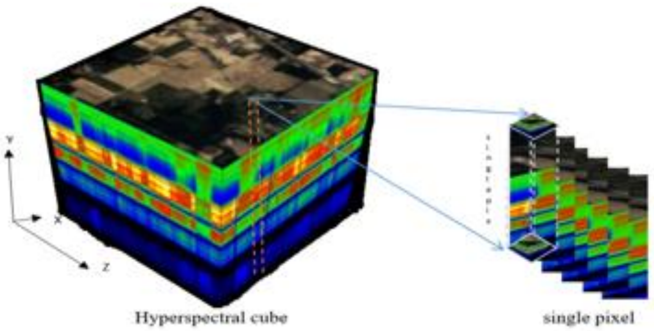

Figure 1. Hyperspectral data cube and spectral-spatial feature

2. PROPOSED METHOD

2.1. Novelty of the method

Convolution neural network is popular for machine learning methods in supervised learning used for the classification of hyperspectral images for feature extraction inspired the hybrid model for classification accuracy. We go over the publically available datasets compared with different methods of the Hybrid 3D convolution neural network (H3D-CNN), based classification technique in-depth in this part and how to educate and evaluate this system on hyperspectral images. The model inspired the state-of-the-art machine learning models for classification of the real-world datasets. Deep learning (DL) techniques are quite capable to represent the extraction of feature information automatically.

2.2. Architecture model evolution

The most accessible approach to retrieve data from an input image is to use a convolution neural network (CNN). When using a 2D-CNN on a hyperspectral image containing hundreds of spectral dimensions, the convolution of each input using kernels might increase the computation cost. As a result, dimensional suppression is used to lower dimensionality before using 2D-CNN to extract features and classification [18].

The principal component analysis (PCA) extracts features from the hyperspectral image to reduce the dimension before 2D-CNN for in-depth features of each pixel with labels [19]. The high-level features are first extracted with the PCA algorithm retaining the spatial information for further classification and loss of spectral information in the 2D-CNN [20]. The PCA reduces the spectral band of the data cube with $\mathbf{C} \in \mathbf{Q}^{\mathbf{WxHxD}}$ where 'C' abide the load, 'W's the measurement (width),' H' is the height and 'D' is the dept out of the spectrum/band, after the reduction of the input data it is $\mathbf{X} \in \mathbf{Q}^{\mathbf{WxHxD}}$ where 'X' is the new modified data input to the convolution neural network with reduced dimensions without losing the spatial information [21]. The data cube is defined as little overlapping patches of the scene, and the truth marks determine the electromagnetic frequency reflected in class labels.

In 2D-CNN, the activation function of the values (x, y) at the j^{th} spatial location at facet maps consisting of i^{th}ply is described as (1) in [22].

$$v_{i,j}^{x,y} = \varphi(b_{i,j} + \sum_{\tau=1}^{d_{l-1}} \sum_{\rho=-\gamma}^{\gamma} \sum_{\sigma=-\delta}^{\delta} \omega_{i,j,\tau}^{\sigma,\rho} * v_{i-1,\tau}^{x+\sigma,y+\rho}) \qquad (1)$$

Where '$b_{i,j}$' bias at 'j^{th}' feature map of the 'i^{th} 'layer, 'ϕ' is the activation function,d_{l-1} endures the feature map for the $(l-1)^{th}$ layer, and the intensity of the kernel is $w_{i,j}$ along with the j^{th} *feature maps* for the i^{th} layer $\gamma+1$ is the width of the kernel $\delta+1$ the height of the kernel and $w_{i,j}$ is the weight parameters of i^{th} layer and j^{th} feature map.

As a result, 3D kernels are employed in 3D convolution procedures to concurrently extract spectral and spatial information for hyperspectral picture categorization [23]. The required information is convolved using learnable 3D kernels 3x3 for each layer in hybrid 3D-CNN [24]. The proposed model with two convolution layers yields the best result. The output of the linear classified layers activated at the activation function is fed to SoftMax [25] to generate the classification image maps.

The 3D-CNN patches split the segments with the filters one in layer-I with a 2x2x9 complex neural network with the stride of '2' and reduce the dimensionality, In layer-II, III in Figure 2. the filters are 3,5 with the stride of '1''2', respectively. In spatial feature mapping, it is convoluted in the fully connected layer, and SoftMax generates the feature maps with reduced predicted output.

$$v_{i,j}^{x,y,z} = \varphi(b_{i,j} + \sum_{\tau=1}^{d_{l-1}} \sum_{\lambda=-\eta}^{\eta} \sum_{\rho=-\gamma}^{\gamma} \sum_{\sigma=-\delta}^{\delta} \omega_{i,j,\tau}^{\sigma,\rho,\lambda} * v_{i-1,\tau}^{x+\sigma,y+\rho,z+\lambda}) \quad (2)$$

3D-CNN activation function and the spatial value position at x, y, z in the j^{th} feature map of the i^{th} layer noted as $v_{i,j}^{x,y,z}$ in (2), the parameters of CNN: such as bias *'b'* weights *'w'* are trained using the supervised approach [26]. The 3D Convolution Neural Network extracts the spatial and spectral, but it increases the computation and complexity [27], also acquiring the advantage of the involuntary element knowledge of 2D and 3D convolutional neural networks. We proposed the fusion spectral convolutions. The 3D-CNN kernel derives spatial and spectral information continuously from HIS datasets in Figure 2.

HSI is volumetric data that has spectral and spatial data with deep, complex dimensions in 3D-CNN [28]. So, we propose the Hybrid 3D-CNN model for deep dimensional spectral analysis and spatial information. The data cube is segmented into the spectral-spatial, applying the PCA to reduce the dimensionality redundancy.

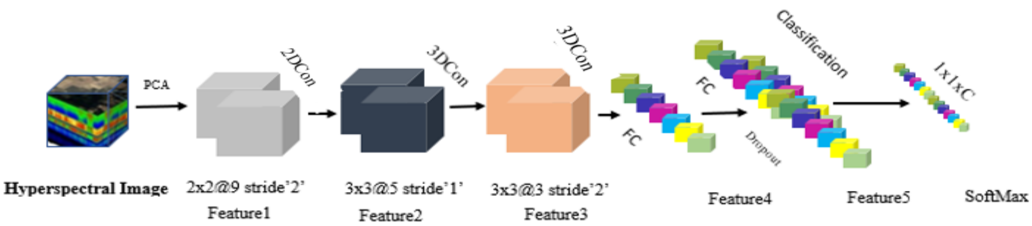

Figure 2. Hybrid 3D-CNN model

2.3. Training model

In convolution neural network HSI samples for 'N' linear different training sample $[(X_i, Y_i)]_{i-1}^{N}$, where $X_i=[x_{i1} \ldots x_{id}]^T \in \mathbb{R}^d$ is the spectral feature of the training samples and $Y_i=[y_{i1} \ldots y_{id}]^T \in \mathbb{R}^d$ label information corresponding to samples X_i, hidden nodes represented as 'L.'

$$f(x) = \sum L\beta g(wi.xj + bi) = Y_j \text{ (I)}$$

Where j=1, $w_i=[w_{i1} \ldots w_{id}]^T$ weight vector linking the i^{th} hidden layer 'b_i'bias of the i^{th} hidden layer,$\beta = [\beta_{i1} \ldots \beta_{im}]^T$ hidden output layer of the neural. There exist realization of the activation function such as sigmoid and radial basis function.

$$g(w, b, x) = 1/(1 + e^{(-(wx+b))})$$

Where equation I is written as H β = Y, Where $\beta = [\beta 1 \ldots \beta L]^T \varepsilon R^{Lxm}$, $Y = [Y_1 \ldots Y_N]^T \varepsilon R^{Nxm}$.

The output of the hidden layer is the combinational coefficient, which balances the spatial and spectral information. The parameters 'μ' are crucial in checking the reliability of hyperspectral image categorization of the picture.

$$\Lambda = \mu Hs + (1 - \mu)Hw$$

Where H_s&H_w are the output of the hidden layer corresponding to the spatial feature and spectral feature for computation, due to the output of the multi-hidden layer in the convolution network of the output is fed with the SoftMax to predict the feature of the classification accuracy.

3. RESULTS AND DISCUSSION

3.1. Data depiction

The sensors collect reflective electromagnetic spectra with narrow spectral bands, this reflective portion creates a unique spectral signature for the classification of objects Our 3D-CNN model can adopt the 3D structure against the start-of-the-art deep learning methods for HIS classification. The publicly available three datasets were used for result analysis and classification.

3.1.1. AVIRIS Indian pines dataset

The dataset of Indian pines was collected aside from airborne in Northwest parts of Indian, USA. It has 16 labeled classes, 10249 samples, and 220 spectral bands. The data set ranges from 0.2 to 2.4 μm wavelength, with a narrow bandwidth. Each scene has 145×145 components with a 20 m spatial declaration. Among 220 bands, 20 noise bands were pre-processed during training [29]. The task of creating ground truth and pixel labeling is time-demanding, and few samples are used for research.

3.1.2. Pavia University (PU) dataset:

Pavia university's images were captured over north Italy. There are 9 design argument precision in the midst of 610 × 610 components, each with a 1.3 m range dimensional declaration of each pixel and removed water-absorbed bands, and the remaining 103 bands are used for training and testing [30]. After removing the noisy and other bands 9 classes have 42776 samples in the dataset used for training. The dataset mainly reflects the urban landscape information.

3.1.3. Salinas dataset:

The AVIRIS sensor was captured in Salinas Valley, California, USA, with a spectral spectrum of 512×217 components, along 224 phantom bands. The statistics from Salinas have a pixel declaration of 3.7 meters and 16 classes.

3.1.4. Kennedy space centre (KSC) dataset

AVIRIS sensors have collected data over the KSC Florida, with 224 strings of 10 nm measurement bands with a core vision of 400-2500 nm, an elevation of around 20 km, and a dimensional decision of approximately 18 m. The records analysis involved 176 posse, elimination of low SNR bands, and water absorption bands.

3.2. Model testing results analysis

Outcomes of the Indian pines scene: The H3D-CNN model in Figure 1 is used to classify each pixel of the 7x7x200 patch. The information included 200 spectral bands handled as channels after the 2D and 3D convolution layers of size 3x3. The step is set to 2,2 in the first function, resulting in hidden layers created from the first to the last stride in the convolution network layers are 5x5,3x3, and 1x1, respectively. Finally, the classified 16 labels are deployed in the image map using SoftMax. The processed model includes the Adam optimizer cross-entropy for the loss function and Relu activation function for the different kernel sizes of the best 3x3. The four layers in the convolution network with different filters of sizes 8,16, and 32, respectively, were used.

The model of Hybrid 3D-CNN is depicted in Figure 2, Table 1 report the different methods used in the different datasets at the different convolution layers Table 1 resemble the results of different methods, the principal component analysis (PCA) lowers the dimensionality of the database without losing spatial data, while the SVM classifier in minimizes the dimensionality of the database without losing spectral information and ignores the spatial and spectral context. The second is that 2D-CNN achieves a comparable performance then SVM and the next is the 3D-CNN method performed well over the other methods in and finally the H3DCNN method achieved the best average accuracy. In Table 2 The kappa assesses the narrowly categorized cases for the model learning, matched with the actual truth and classified maps, regulating the accuracy with different methods and the average accuracy (AA) and overall accuracy (OA) for different methods. Figure 3 and Figure 4 show the classified outcomes for the IP dataset and the SA dataset, respectively, and the accuracy of each class label is presented in the Table 1.

Table 1. Classification accuracy of Indian Pines, Salinas dataset comparisons

S.NO	Class Labels	No. Samples	Indian_ Pines Accuracy				Class Labels	No. Samples	Salinas DS Accuracy			
			H3D-CNN	3D-CNN	2D-CNN	SVM			H3D-CNN	3D-CNN	2D-CNN	SVM
1	Alfalfa	46	88.90	85.71	71.72	85.71	Brocoli-green-weeds-1	804	100	97.50	99.50	99.83
2	Corn-notill	1428	92.11	96.46	95.85	86.82	Brocoli-green-weeds-2	1490	100	99.46	99.82	100
3	Corn-mintill	830	96.08	97.13	95.90	86.12	Fallow	790	100	97.80	98.31	100
4	Corn	237	97.90	98.55	73.91	88.40	Fallow-rough-plow	558	99.73	97.13	97.61	99.04
5	Grass-pasture	483	87.33	97.90	97.20	95.10	Fallow-smoth	1071	99.85	98.80	98.50	99.75
6	Grass-trees	730	99.82	97.68	96.31	98.61	Stubble	1584	100	98.91	99.75	100
7	Grass-pasture-mowed	28	81.81	100	100	75.00	Celery	1432	99.75	96.55	98.42	99.91
8	Hay-windrowed	478	100	99.30	100	98.60	Grapes-untrained	4509	95.80	97.28	99.47	92.69
9	Oats	20	100	100	100	100	Soil-vinyard-develop	2481	99.97	99.84	99.89	100
10	Soybeans-notill	972	90.23	98.26	97.20	87.19	Corn-sensed-green-weeds	1311	98.24	98.78	99.70	99.08
11	Soybean-mintill	2455	97.80	98.77	99.04	91.01	Lettuce-romaine-4wk	427	99.64	99.06	99.37	100
12	Soybean-clean	593	98.10	97.15	95.45	94.84	Lettuce-romaine-5k	771	100	99.14	98.09	100
13	Wheat	205	88.96	96.72	100	100	Lettuce-romaine-6k	366	100	90.55	96.00	99.64
14	Wood	1265	99.02	99.46	98.94	96.81	Lettuce-romaine-7k	428	98.94	93.46	96.89	98.75
15	Buildings-Grass-Trees-Drives	386	96.08	93.80	94.73	81.57	Vinyard-untrained	2907	95.23	97.47	99.22	82.61
16	Stone-steel-Towers	93	97.03	100	100	100	Vinyard-vertical-trellis	723	99.58	99.06	99.41	99.82
		10249						54129				
AA			97.53	97.31	96.37	85.23	AA		99.85	98.65	98.90	97.37
OA			98.29	98.92	97.08	86.55	OA		99.67	99.08	98.96	94.95

Table 2. Classification accuracy of different methods

Methods	Indian pines dataset			Salinas dataset		
	OA	AA	Kappa	OA	AA	Kappa
SVM	85.30	79.03	83.10	92.95	94.60	92.11
2D-CNN	89.48	86.14	87.96	97.38	98.84	97.08
3D-CNN	91.10	91.58	89.98	93.96	97.01	93.32
H3D-CNN	98.30	96.53	98.06	99.67	99.85	99.64

The training and validations of the datasets were analyzed at a loss, and accuracy compared with 50 to 100 epochs of the datasets in the fully connected layersr1 and layer 2. We used 256 units for batch size for an activation dropout rate of 0.4%. For the Indian pines and Salinas datasets, all the analyses are in Table 2 display the findings for several techniques in terms of AA, OA, and kappa coefficient. The performance of the multiple databases, and the spectral and spatial information of the 3D-CNN and the 2D-CNN, are comparable.

The Indian pines and Salinas classification map of the hyperspectral image are shown in Figure 3 and Figure 4. We used SVM, 2D-CNN, 3D-CNN, [30], and H3D-CNN methods. The quality of the H3D-CNN classified image is better than the other models. The spectral accuracy of class label information of different datasets shown in Figure 5.

The confusion matrix of the Salinas classified hyperspectral image is shown in Figure 6. The accuracy and loss convergence of 50 epochs of training and validation are shown in Figure 7. The computation efficiency of the H3D-CNN in terms of the training and testing with the window size 25x25 is the best outcome of spatial dimensions compact to model with the 10% of the samples used for the summarization for the best results.

We have trained our model using Keras, Scikit, and Tensorflow, and it is trained on a single AMD Radeon 1.60 GHz 4GB GPU and Google Colab. We have compared our results with SVM, 2D-CNN, 3D-CNN, and H3D-CNN. Table 1 summarises the accuracy and performance of the Indian Pines (IP), Pavia University (PU), and Salinas (SA) datasets. The grades of AA and OA used for altered approaches precision adjacent to an evaluation of instruction and test outcomes are 98.53 %(AA), 98.29 %(OA) for Indian Pines, and 99.67% (AA), 99.85% (OA) for Salinas data with 50 epochs for data training. We have illustrated this in Table.2, the spatial performance of the H3D-CNN model with 19 x 19 spatial dimensions are used for the proposed model, and computed the results with training data only10% of the total samples. Where the proposed model still outperforms other methods.

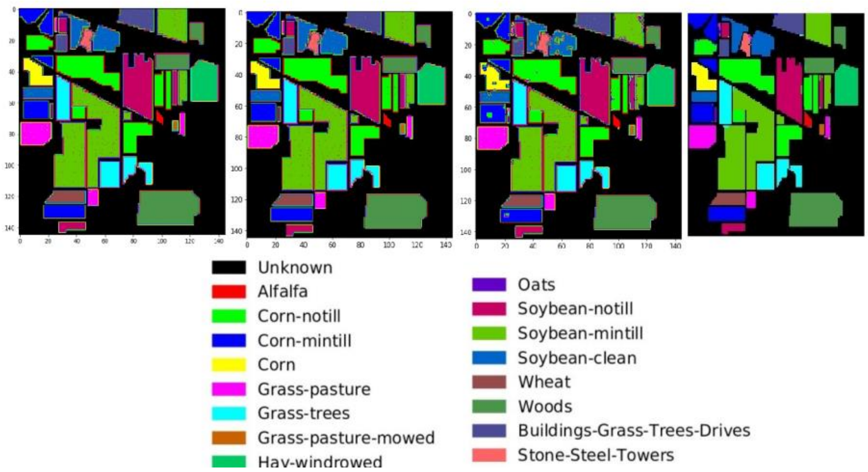

Figure 3. The Indian Pines classification SVM, 2D-CNN, 3D-CNN, H3D-CNN predicted map with labels

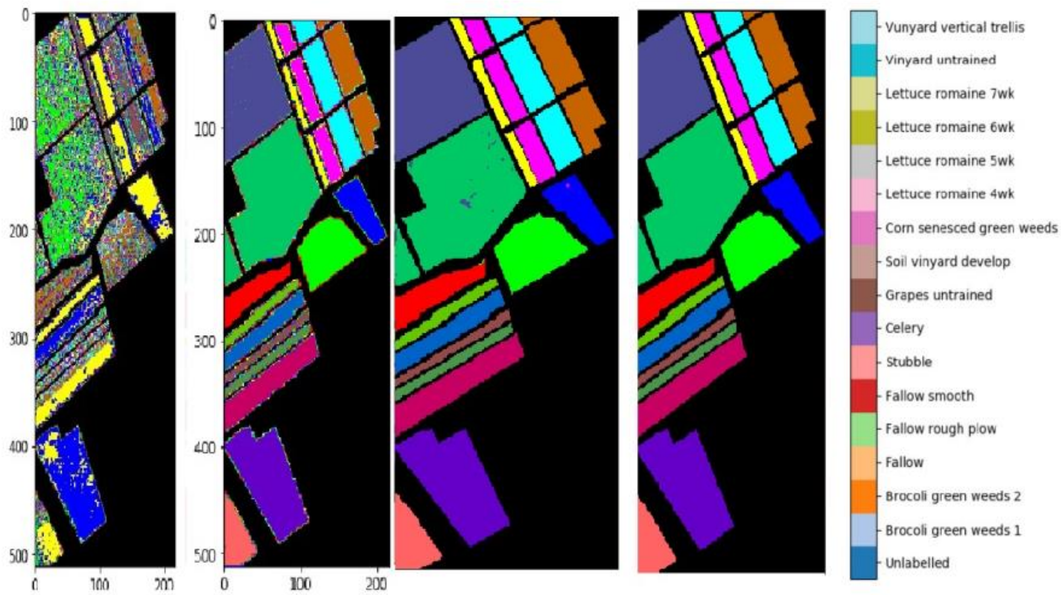

Figur 4. Salinas classification SVM, 2D-CNN, 3D-CNN, H3D-CNN predicted map with labels

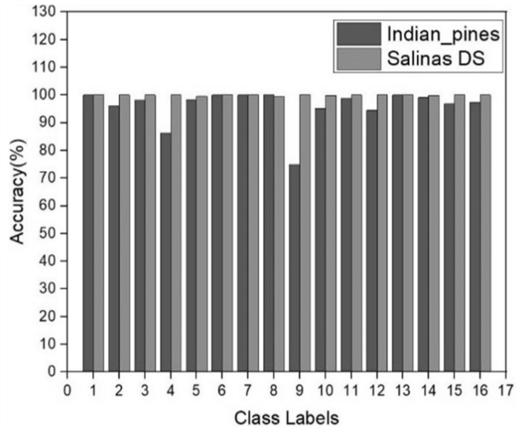

Figure 5. Indian Pines, Salinas accuracy

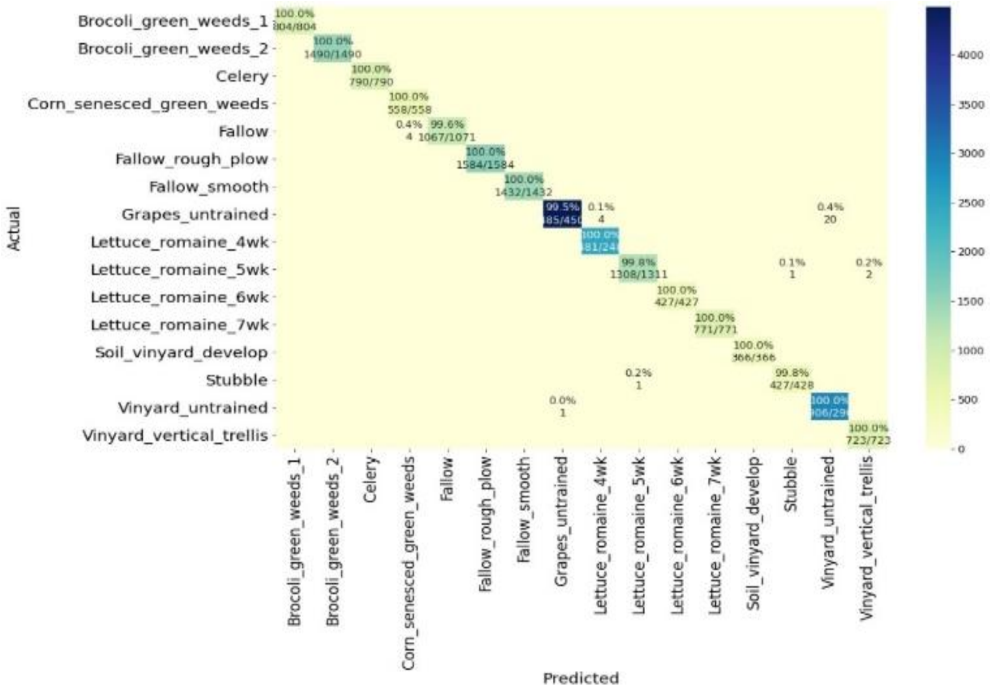

Figure 6. Confusion matrix of the salinas dataset

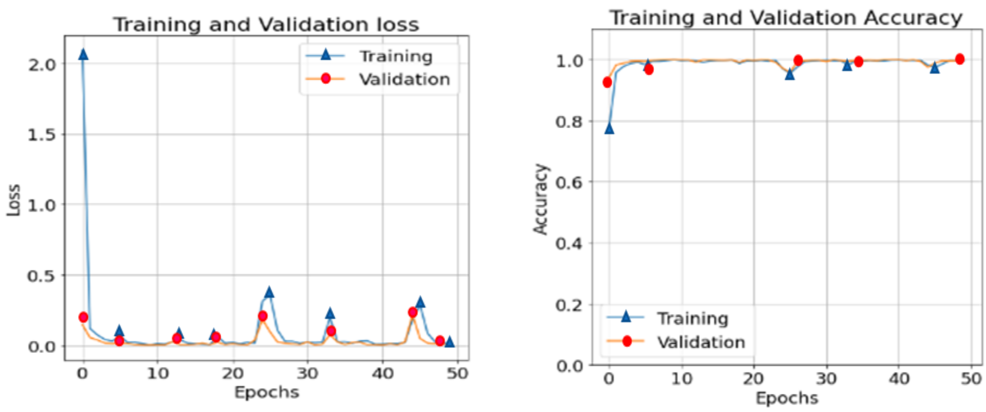

Figure 7. Salinas datasets training and validation loss and accuracy

4. CONCLUSION

This paper proposes a HIS classification architecture with a reduced-dimensional Hybrid 3D-CNN model, demonstrating the overall performance for data training and research. The H3D-CNN framework suggested the exclusive use of classified spatial and spectral knowledge for HSI analysis. In future studies, we intend to explore theoretically more powerful HSI classification approaches based on H3D-CNN that can be used for unlabelled samples. Untreated samples are much simpler to access in HSI than labeled samples. To allow better use of such unmarked samples, including in the organized categorization process relating to 3D-CNN files, the 3D convolution spectral classification method based on 3D-CNN wishes to be enhanced.

REFERENCES

[1] J. M. Bioucas-Dias, A. Plaza, G. Camps-Valls, P. Scheunders, N. M. Nasrabadi, and J. Chanussot, "Hyperspectral remote sensing data analysis and future challenges," *IEEE Geoscience and Remote Sensing Magazine*, vol. 1, no. 2, pp. 6–36, Jun. 2013, doi: 10.1109/MGRS.2013.2244672.

[2] M. Chi and L. Bruzzone, "Semisupervised classification of hyperspectral images by SVMs optimized in the primal," *IEEE Transactions on Geoscience and Remote Sensing*, vol. 45, no. 6, pp. 1870–1880, Jun. 2007, doi: 10.1109/TGRS.2007.894550.

[3] F. Melgani and L. Bruzzone, "Classification of hyperspectral remote sensing images with support vector machines," *IEEE Transactions on Geoscience and Remote Sensing*, vol. 42, no. 8, pp. 1778–1790, Aug. 2004, doi: 10.1109/TGRS.2004.831865.

[4] J. Li, J. M. Bioucas-Dias, and A. Plaza, "Spectral-spatial hyperspectral image segmentation using subspace multinomial logistic regression and Markov random fields," *IEEE Transactions on Geoscience and Remote Sensing*, vol. 50, no. 3, pp. 809–823, Mar. 2012, doi: 10.1109/TGRS.2011.2162649.

[5] J. Li, J. M. Bioucas-Dias, and A. Plaza, "Semisupervised hyperspectral image classification using soft sparse multinomial logistic regression," *IEEE Geoscience and Remote Sensing Letters*, vol. 10, no. 2, pp. 318–322, Mar. 2013, doi: 10.1109/LGRS.2012.2205216.

[6] Y. Zhong and L. Zhang, "An adaptive artificial immune network for supervised classification of multi-/hyperspectral remote sensing imagery," *IEEE Transactions on Geoscience and Remote Sensing*, vol. 50, no. 3, pp. 894–909, Mar. 2012, doi: 10.1109/TGRS.2011.2162589.

[7] H. Jiao, Y. Zhong, and L. Zhang, "Artificial DNA computing-based spectral encoding and matching algorithm for hyperspectral remote sensing data," *IEEE Transactions on Geoscience and Remote Sensing*, vol. 50, no. 10 PART2, pp. 4085–4104, Oct. 2012, doi: 10.1109/TGRS.2012.2188856.

[8] A. Santara *et al.*, "Bass net: Band-adaptive spectral-spatial feature learning neural network for hyperspectral image classification," *IEEE Transactions on Geoscience and Remote Sensing*, vol. 55, no. 9, pp. 5293–5301, Sep. 2017, doi: 10.1109/TGRS.2017.2705073.

[9] Y. LeCun, L. Bottou, Y. Bengio, and P. Haffner, "Gradient-based learning applied to document recognition," *Proceedings of the IEEE*, vol. 86, no. 11, pp. 2278–2323, 1998, doi: 10.1109/5.726791.

[10] Y. Chen, Z. Lin, X. Zhao, G. Wang, and Y. Gu, "Deep learning-based classification of hyperspectral data," *IEEE Journal of Selected Topics in Applied Earth Observations and Remote Sensing*, vol. 7, no. 6, pp. 2094–2107, Jun. 2014, doi: 10.1109/JSTARS.2014.2329330.

[11] C. Szegedy *et al.*, "Going deeper with convolutions," in *Proceedings of the IEEE Computer Society Conference on Computer Vision and Pattern Recognition*, Jun. 2015, vol. 07-12-June-2015, pp. 1–9, doi: 10.1109/CVPR.2015.7298594.

[12] W. Hu, Y. Huang, L. Wei, F. Zhang, and H. Li, "Deep convolutional neural networks for hyperspectral image classification," *Journal of Sensors*, vol. 2015, pp. 1–12, 2015, doi: 10.1155/2015/258619.

[13] Z. Zuo *et al.*, "Learning vontextual dependence with convolutional hierarchical recurrent neural networks," *IEEE Transactions on Image Processing*, vol. 25, no. 7, pp. 2983–2996, Jul. 2016, doi: 10.1109/TIP.2016.2548241.

[14] Z. Zhong, J. Li, Z. Luo, and M. Chapman, "Spectral-spatial residual network for hyperspectral image classification: A 3-D deep learning framework," *IEEE Transactions on Geoscience and Remote Sensing*, vol. 56, no. 2, pp. 847–858, Feb. 2018, doi: 10.1109/TGRS.2017.2755542.

[15] L. Fang, Z. Liu, and W. Song, "Deep hashing neural networks for hyperspectral image feature extraction," *IEEE Geoscience and Remote Sensing Letters*, vol. 16, no. 9, pp. 1412–1416, Sep. 2019, doi: 10.1109/lgrs.2019.2899823.

[16] M. He, B. Li, and H. Chen, "Multi-scale 3D deep convolutional neural network for hyperspectral image classification," in *Proceedings - International Conference on Image Processing, ICIP*, Sep. 2018, vol. 2017-September, pp. 3904–3908, doi: 10.1109/ICIP.2017.8297014.

[17] S. H. S. Basha, S. Ghosh, K. K. Babu, S. R. Dubey, V. Pulabaigari, and S. Mukherjee, "RCCNet: An efficient convolutional neural network for histological routine colon cancer nuclei classification," in *2018 15th International Conference on Control, Automation, Robotics and Vision, ICARCV 2018*, Nov. 2018, pp. 1222–1227, doi: 10.1109/ICARCV.2018.8581147.

[18] V. K. Repala and S. R. Dubey, "Dual CNN models for unsupervised monocular depth estimation," in *Lecture Notes in Computer Science (including subseries Lecture Notes in Artificial Intelligence and Lecture Notes in Bioinformatics)*, vol. 11941 LNCS, 2019, pp. 209–217.

[19] C. Nagpal and S. R. Dubey, "A performance evaluation of convolutional neural networks for face anti spoofing," in *Proceedings of the International Joint Conference on Neural Networks*, Jul. 2019, vol. 2019-July, pp. 1–8, doi: 10.1109/IJCNN.2019.8852422.

[20] X. Kang, B. Zhuo, and P. Duan, "Dual-path network-based hyperspectral image classification," *IEEE Geoscience and Remote Sensing Letters*, vol. 16, no. 3, pp. 447–451, Mar. 2019, doi: 10.1109/LGRS.2018.2873476.

[21] Y. Yu, Z. Gong, C. Wang, and P. Zhong, "An unsupervised convolutional feature fusion network for deep representation of remote sensing images," *IEEE Geoscience and Remote Sensing Letters*, vol. 15, no. 1, pp. 23–27, 2018, doi: 10.1109/LGRS.2017.2767626.

[22] W. Li, C. Chen, M. Zhang, H. Li, and Q. Du, "Data augmentation for hyperspectral image classification with deep CNN," *IEEE Geoscience and Remote Sensing Letters*, vol. 16, no. 4, pp. 593–597, Apr. 2019, doi: 10.1109/LGRS.2018.2878773.

[23] W. Song, S. Li, L. Fang, and T. Lu, "Hyperspectral image classification with deep feature fusion network," *IEEE Transactions on Geoscience and Remote Sensing*, vol. 56, no. 6, pp. 3173–3184, Jun. 2018, doi: 10.1109/TGRS.2018.2794326.

[24] G. Cheng, Z. Li, J. Han, X. Yao, and L. Guo, "Exploring hierarchical convolutional features for hyperspectral image classification," *IEEE Transactions on Geoscience and Remote Sensing*, vol. 56, no. 11, pp. 6712–6722, Nov. 2018, doi: 10.1109/TGRS.2018.2841823.

[25] J. M. Haut, S. Bernabé, M. E. Paoletti, R. Fernandez-Beltran, A. Plaza, and J. Plaza, "Low-high-power consumption architectures for deep-learning models applied to hyperspectral image classification," *IEEE Geoscience and Remote Sensing Letters*, vol. 16, no. 5, pp. 776–780, May 2019, doi: 10.1109/LGRS.2018.2881045.
[26] Y. Chen, H. Jiang, C. Li, X. Jia, and P. Ghamisi, "Deep feature extraction and classification of hyperspectral images based on convolutional neural networks," *IEEE Transactions on Geoscience and Remote Sensing*, vol. 54, no. 10, pp. 6232–6251, Oct. 2016, doi: 10.1109/TGRS.2016.2584107.
[27] X. Mei *et al.*, "Spectral-spatial attention networks for hyperspectral image classification," *Remote Sensing*, vol. 11, no. 8, 2019, doi: 10.3390/rs11080920.
[28] L. Mou, P. Ghamisi, and X. X. Zhu, "Unsupervised spectral-spatial feature learning via deep residual conv-deconv network for hyperspectral image classification," *IEEE Transactions on Geoscience and Remote Sensing*, vol. 56, no. 1, pp. 391–406, Jan. 2018, doi: 10.1109/TGRS.2017.2748160.
[29] M. E. Paoletti, J. M. Haut, R. Fernandez-Beltran, J. Plaza, A. J. Plaza, and F. Pla, "Deep pyramidal residual networks for spectral-spatial hyperspectral image classification," *IEEE Transactions on Geoscience and Remote Sensing*, vol. 57, no. 2, pp. 740–754, Feb. 2019, doi: 10.1109/TGRS.2018.2860125.
[30] M. E. Paoletti *et al.*, "Capsule Networks for Hyperspectral Image Classification," *IEEE Transactions on Geoscience and Remote Sensing*, vol. 57, no. 4, pp. 2145–2160, Apr. 2019, doi: 10.1109/TGRS.2018.2871782.

BIOGRAPHIES OF AUTHORS

Easala Ravi Kondal is received his M.Tech. in Computer Science & Engineering from Jawaharlal Nehru Technological University, Hyderabad, India, and he is pursuing a Ph.D. from VIT-AP University Amaravati, Andhra Pradesh, India, from 2017. Research area interests are Digital Image processing, computer vision, and Machine Learning. He can be contacted at email: easala.ravi@vitap.ac.in.

Dr. Soubhagya Sankar Barpanda is an Associate Professor at the Department of Computer Science & Engineering, VIT-AP University, Amaravati, India. He received his doctoral degree from the Department of Computer Science & Engineering, National Institute of Technology Rourkela, India. He has completed his M. Tech. Degree from the same institute. His research interests include biometric security, Digital Image processing, computer vision, and Machine Learning. He can be contacted at email: soubhagya.barpanda@vitap.ac.in.